Generalized Unsteady Embedded Newtonian Flow

Lars E. Ericsson*
Lockheed Missiles & Space Company, Inc., Sunnyvale, Calif.

An analysis is presented which extends the previously developed unsteady embedded Newtonian theory down to finite supersonic Mach numbers. It is found that Mach number can have a very large influence on the stability characteristics of slender blunted cones, and that there exist cone angle-nose bluntness combinations for which these Mach number effects are minimized. The computed effects of nose bluntness on static and dynamic stability derivatives are in excellent agreement with available experimental data. This also holds true for the highly nonlinear effects of angle of attack.

Nomenclature

a = speed of sound
A_1, A_2 = constants defining f^*, Eq. (6)
ΔA = surface area element
c = reference length, cylinder or base diameter
d_B = base diameter
d_N = nose (bluntness) diameter
D_N = nose drag
Coef. C_{D_N} = $D_N / (\rho_\infty U_\infty^2/2)(\pi d_N^2/4)$
f = pressure correlation function, $f = 2f^*$
f^* = dynamic pressure ratio, $f^* = \rho U^2/\rho_\infty U_\infty^2$
g^* = velocity ratio, $g^* = U/U_\infty$
ℓ = sharp cone body length
M = Mach number, $M = U/a$
M_p = pitching moment
coef. C_m = $M_p / (\rho_\infty U_\infty^2/2)\,Sc$
p = static pressure
coef. C_p = $(p - p_\infty) / (\rho_\infty U_\infty^2/2)$
p_0 = blast wave pressure
coef. C_{p_0} = $(p_0 - P_\infty) / (\rho_\infty U_\infty^2/2)$
q = rigid body pitch rate
$\bar{q}$ = dynamic pressure $\bar{q} = \rho U^2/2$
r = body radius (see Fig. 1)
R = radial distance from bow shock centerline (see Fig. 1)
Re = Reynolds number, $\mathrm{Re}_{\ell\infty} = \ell U\infty/\nu_\infty$
S = reference area, $S = \pi c^2/4$
t = time
U = axial velocity
$V_\perp$ = velocity normal to body surface
x = axial coordinate (see Fig. 1)
x_0 = centroid location of equivalent sphere representing blunt nose ($x_0 = 0$ for spherical nose bluntness)
$\Delta\bar{x}$ = cone center of gravity location forward of base
z = translatory coordinate (see Fig. 1)
α = angle of attack
β = angular body coordinate (see Fig. 1)
γ = ratio of specific heats ($\gamma = 1.4$ for air)
θ = body perturbation in pitch
θ_c = cone half-angle
ν = kinematic viscosity of air
ρ = air density
ϕ = azimuth (see Fig. 1)
χ^*, χ = hypersonic similarity parameters defined in Eqs. (1) and (5), respectively ($\chi^* = \chi$ when $\alpha = 0$)

Subscripts

B = base
BW = blast wave
c = cone
CG = center of gravity or oscillation center
N = nose
NEWT = Newtonian value
sh = bow shock
∞ = freestream conditions

Derivative Symbols

$\dot{\theta}$ = $\partial\theta/\partial t$
C_{N_α} = $\partial C_N/\partial\alpha$ $\quad C_{m_i} = \partial C_m/\partial\theta$
C_{m_q} = $\partial C_m/\partial(cq/U_\infty)$ $\quad C_{m_{\dot\alpha}} = \partial C_m/\partial(c\dot\alpha/U_\infty)$
C_{m_θ} = $C_{m_q} + C_{m_{\dot\alpha}}$

Introduction

SIMPLE Newtonian theory[1] has provided an indispensible tool for hypersonic vehicle design. It works well as long as the bow shock follows the body contour very closely, as is the case for pointed bodies and for very blunt geometries. However, in the case of slender, blunted cones the Newtonian theory gives prohibitively large errors. Until recent-

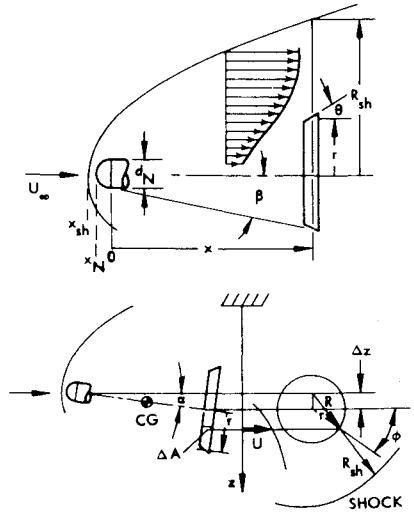

Fig. 1 Bow-shock induced inviscid shear flow at near zero angle of attack.

Received February 10, 1975; revision received June 16, 1975. The paper is based mainly upon results obtained in a study made for Naval Air Development Center, Warminster, Pa., Contract N62269-73C-0713, under the direction of Dr. A. Somoroff. The author gratefully acknowledges the assistance of N. Davis in developing the needed computer program.

Index categories: Supersonic and Hypersonic Flow; Nonsteady Aerodynamics; Entry Vehicles Dynamics and Control.

*Consulting Engineer. Associate Fellow AIAA.

ly only costly numerical methods [2] could provide the correct unsteady aerodynamic characteristics for slender blunted cones. The recently developed unsteady embedded Newtonian theory gives prohibitively large errors. Until recently only costly numerical methods[2] could provide the correct unsteady aerodynamic characteristics for slender needed accuracy.[4] In this paper the restriction to hypersonic Mach numbers is removed and an analytic theory is provided that can compute the effect of nose bluntness for Mach numbers down to $M_\infty = 3$.

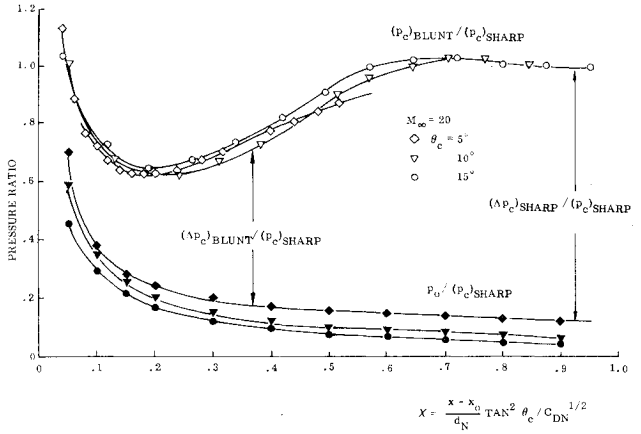

Fig. 2 Pressure distribution over blunted slender bodies of revolution at $M_\infty = 20$.

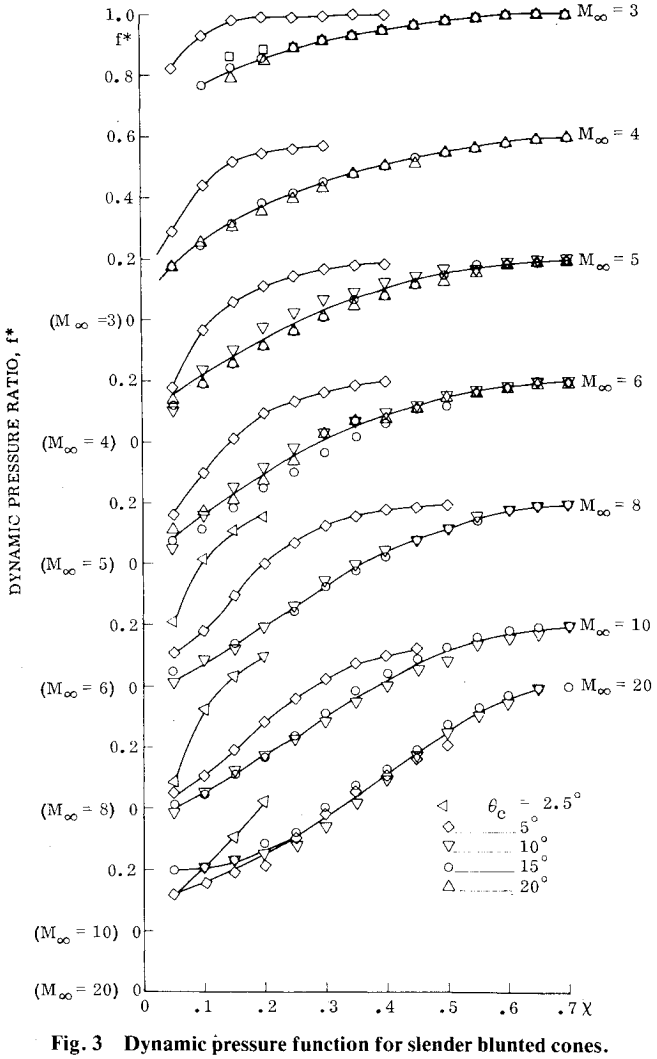

Fig. 3 Dynamic pressure function for slender blunted cones.

Embedded Newtonian Flow

In the embedded Newtonian flow concept first proposed by Sieff,[5] Newtonian theory is used in the nonuniform, inviscid flowfield defined by the bow shock.[6] The shock shape is defined by the nose bluntness and can be related to the nose drag.[7] In Ref. 3, the original concept by Sieff is extended to include the effects of entropy gradient and convective time lag on the hypersonic unsteady aerodynamics of slender blunted cones and cylinder-flare configurations. This unsteady embedded Newtonian theory is modified here to account for the effect of finite Mach number, $M_\infty \neq \infty$.

Generalized Embedded Newtonian Flow

It has been shown that, through appropriate modification, the blast-wave parameters can be extended to the correlation of bluntness-induced pressures on cones and wedges.[8-11] For slender cones (θ_c small) in air ($\gamma = 1.4$) the result obtained for $M_\infty = \infty$ is[3]

$$C_p = (C_p)_{BW} + (C_p)_{NEWT} f^*(\chi^*) \tag{1a}$$

$$\chi^* = \left[\frac{R}{d_N} - \frac{1}{2} \right]^2 / C_{D_N}{}^{1/2} \left[\frac{x}{d_N} - \frac{x_N}{d_N} \right] \tag{1b}$$

$$\left[\frac{R}{d_N} \right]^2 = \left[\frac{\Delta z}{d_N} \right]^2 + 2 \frac{\Delta z}{d_N} \cos\alpha \left[\frac{1}{2} + \frac{x}{d_N} \tan\theta_c \right] \sin\phi + \left[\frac{1}{2} + \frac{x}{d_N} \tan\theta_c \right]^2 [\cos^2\alpha \sin^2\phi + \cos^2\phi] \tag{1c}$$

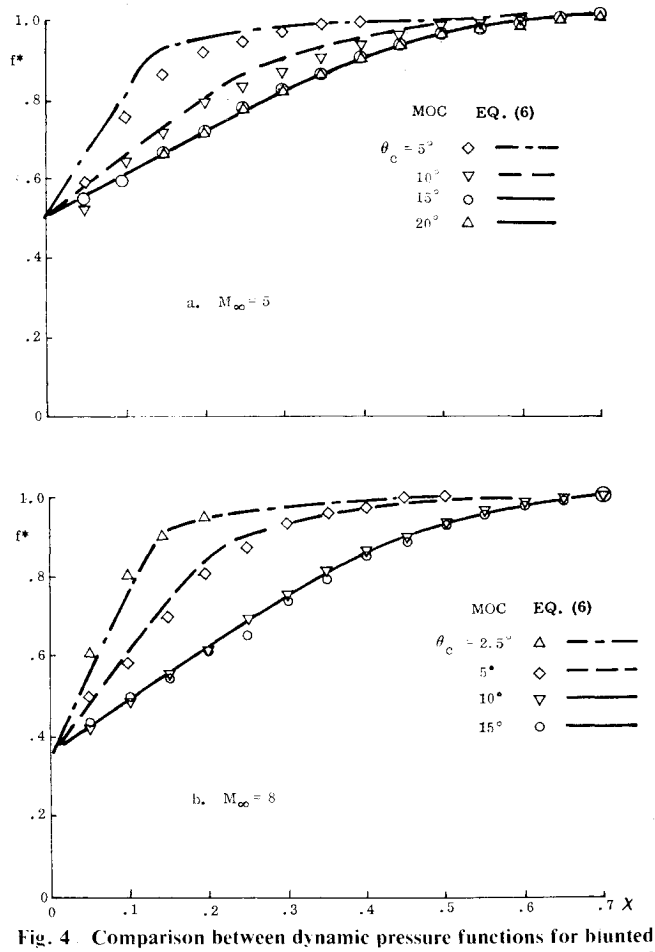

Fig. 4 Comparison between dynamic pressure functions for blunted slender cones as determined by analytic approximation and Method Of Characteristics.

For the spherical nose bluntness considered in the present analysis $x_N/d_N = -\frac{1}{2}$. When defining f^* for finite Mach numbers $x_{sh} = 0$ is assumed for simplicity. This is permissible as the analytic approximation of f^* is obtained by subtracing the blast-wave contribution from the pressures defined by the Method of Characteristics (MOC).[12]

The theoretical pressure distributions computed by the (MOC)[12] at $M_\infty = 20$ for spherically blunted 5°, 10°, and 15°-cones are shown in Fig. 2 in form of $C_p/(C_p)_{NEWT}$. Also shown in this form are the blast-wave pressures for hemisphere cylinders using Kuehn's correlation.[13] The difference between cone pressures and blast-wave pressures is a measure of the dynamic pressure profile in the "entropy wake"[3]

$$f^*(\chi) = \bar{q}/\bar{q}_\infty = (\Delta p_c)_{BLUNT}/(\Delta p_c)_{SHARP} \qquad (2)$$

The f^* function defined in this manner is shown in Fig. 3 for $2.5° \le \theta_c \le 20°$, $3 \le M_\infty \le 20$. The expected collapse of the pressure distribution curves occurs only for cone angles above a critical value. Closer examination reveals that the critical value is the freestream Mach angle. Including the Mach angle in the shock-angle/cone-angle chart of Ref. 14 indicates that, when the cone angle "dips below" μ, the shock angle remains more or less insensitive to θ_c. In the limit, when $\theta_c \ll \mu$, the shock angle is completely independent of θ_c. Figure 3 shows that the entropy profile is becoming steeper as θ_c is decreased. A steepening of the profile is also observed when going from blunted cones to blunted cylinder-flare bodies.[3] At hypersonic speeds the f^* function for blunted cylinder-flare bodies is[3]

$$f^* = 0.17 + 2.75\chi^* + 4\chi^{*2} \qquad (3)$$

and for blunted cones Note that $f = 2f^*$.

$$f^* = \begin{cases} 0.17 + 1.375\,\chi^* & : \chi^* \le 0.49 \\ 1 - 3.43(0.7 - \chi^*)^2 & : 0.49 < \chi^* < 0.7 \\ 1 & : 0.7 \le \chi^* \end{cases} \qquad (4)$$

For $\alpha = 0$, $\chi^* = \chi$, where the similarity parameter χ can be written

$$\chi = [(x - x_N)/d_N]\,[\tan^2\beta/C_{D_N}^{1/2}] \qquad (5)$$

$\beta = \theta_c$ for the blunted cone (see Fig.1). The following "analytic curve fit" for blunted slender cones is obtained

$$\theta_c/\mu \ge 1 : f^* = \begin{cases} f_0^* + B\,\chi^* & : \chi^* \le \chi^*_1 \\ 1 - k_f(\chi_0^* - \chi^*)^2 & : \chi_1^* < \chi^* < \chi_0^* \\ 1 & : \chi_0^* \le \chi^* \end{cases} \qquad (6a)$$

$$\theta_c/\mu < 1 : f^* = \begin{cases} f_0^* + AB\,\chi^* & : \chi^* \le \chi_2^* \\ 1 - b\{1 - \{1 - [(\chi_0^* - \chi^*)/a]^2\}^{1/2}\} & : \chi_2^* < \chi^* < \chi_0^* \\ 1 & : \chi_0^* \le \chi^* \end{cases} \qquad (6b)$$

$$\chi_0^* = 0.7 \quad \chi_1^* = 2\chi^*_{crit} - \chi_0^*; \qquad \chi^*_{crit} = (1 - f_0^*)/AB \qquad (6c)$$

$$\chi_2^* = (f_1^* - f_0^*)/AB; \qquad f_1^* = 0.9 - [(3.33 - A)/2.33]\,(0.9 - f_2^*) \qquad (6d)$$

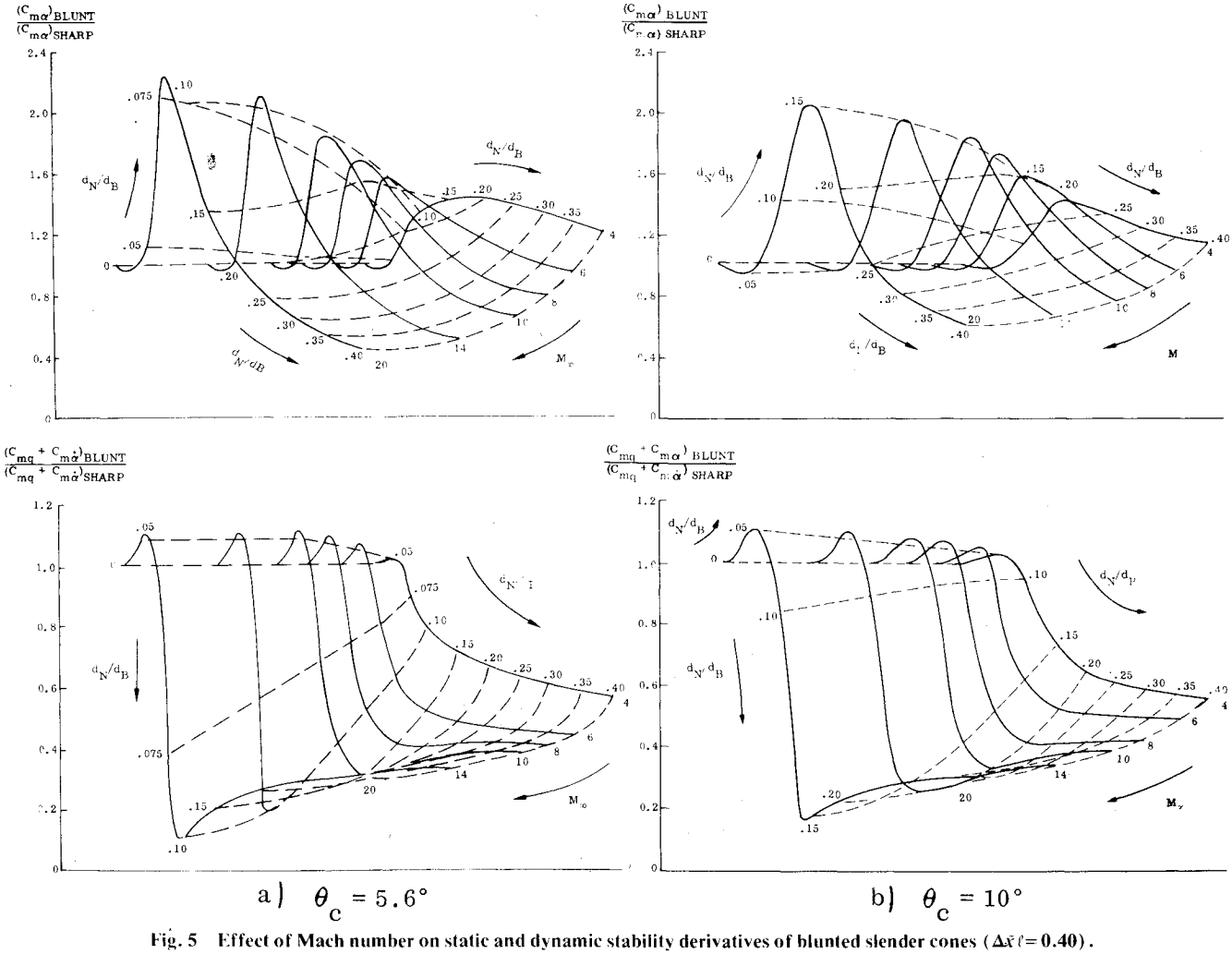

Fig. 5 Effect of Mach number on static and dynamic stability derivatives of blunted slender cones ($\Delta\bar{x}' = 0.40$).

$$f_2^* = f_0^* + AB\chi_3^*; \quad \chi_3^* = \chi_1^* + 0.01 \tag{6e}$$

$$k_f = B/2(\chi_0^* - \chi_1^*) \tag{6f}$$

$$f_0^* = 0.165 + [9.65/(M_\infty + 8.7)]^3 : M_\infty \geq 3 \tag{6g}$$

$$B = \begin{cases} 1.375 - 0.5[0.17(10 - M_\infty)]^3 & : 3 \leq M_\infty < 10 \\ 1.375 & : M_\infty \geq 10 \end{cases} \tag{6h}$$

$$A = \begin{cases} 3.33 & : \theta_c^*/\mu \leq 0.23 \\ 3.33 - 3.03[(\theta_c^*/\mu) - 0.23] & : 0.23 < \theta_c^*/\mu < 1 \\ 1 & : 1 \leq \theta_c^*/\mu \end{cases} \tag{6i}$$

$$a = (\chi_0^* - \chi_2^*)\left\{1 + \left[\frac{(1 - f_1^*)}{(\chi_0^* - \chi_2^*)AB}\right]^2 \Big/ \left[1 - \frac{2(1 - f_1^*)}{(\chi_0^* - \chi_2^*)AB}\right]\right\}^{1/2} \tag{6j}$$

$$b = (1 - f_1^*)\left\{1 + \frac{(1 - f_1^*)}{(\chi_0^* - \chi_2^*)AB} \Big/ \left[1 - \frac{2(1 - f_1^*)}{(\chi_0^* - \chi_2^*)AB}\right]\right\} \tag{6k}$$

$$\theta_c^* = \theta_c \text{ for } \alpha = 0 \tag{6l}$$

For $\theta_c/\mu \geq 1$ and $M_\infty = \infty$, Eqs. (6) reduce to Eqs. (4), as they should.

A comparison between predictions through Eq. (6) and MOC-computations is made in Fig. 4 for $M_\infty = 5$ and $M_\infty = 8$. In addition to the dynamic pressure profile approximation given by Eq. (6) the velocity profile is needed for the computation of convective time lag.[3] Through reasoning analogous to that for hypersonic flow conditions,[3] the approximation for the velocity ratio is as follows

$$g^*(\chi^*) = U/U_\infty = \begin{cases} g_0 + k_g \chi^{*1/2} & : \chi^* < \chi_{crit}^* \\ 1 & : \chi_{crit}^* \leq \chi^* \end{cases} \tag{7a}$$

$$k_g = \{0.304\, B/[1 + (3.33 - A)/2.33]\}^{1/2} \tag{7b}$$

$$g_0^* = 1 - k_g \chi_{crit}^* \tag{7c}$$

When $\alpha \neq 0$, θ_c^* is defined using the tangent cone approximation

$$\theta_c^* = \sin^{-1}(V_\perp/U) \tag{8a}$$

$$V_\perp/U = \cos\alpha \sin\theta_c + \sin\alpha \cos\theta_c \sin\phi \tag{8b}$$

Discussion of Results

Incorporating Eqs. (6-8) in the embedded Newtonian analysis of Ref. 3 gives the results shown in Fig. 5. It can be

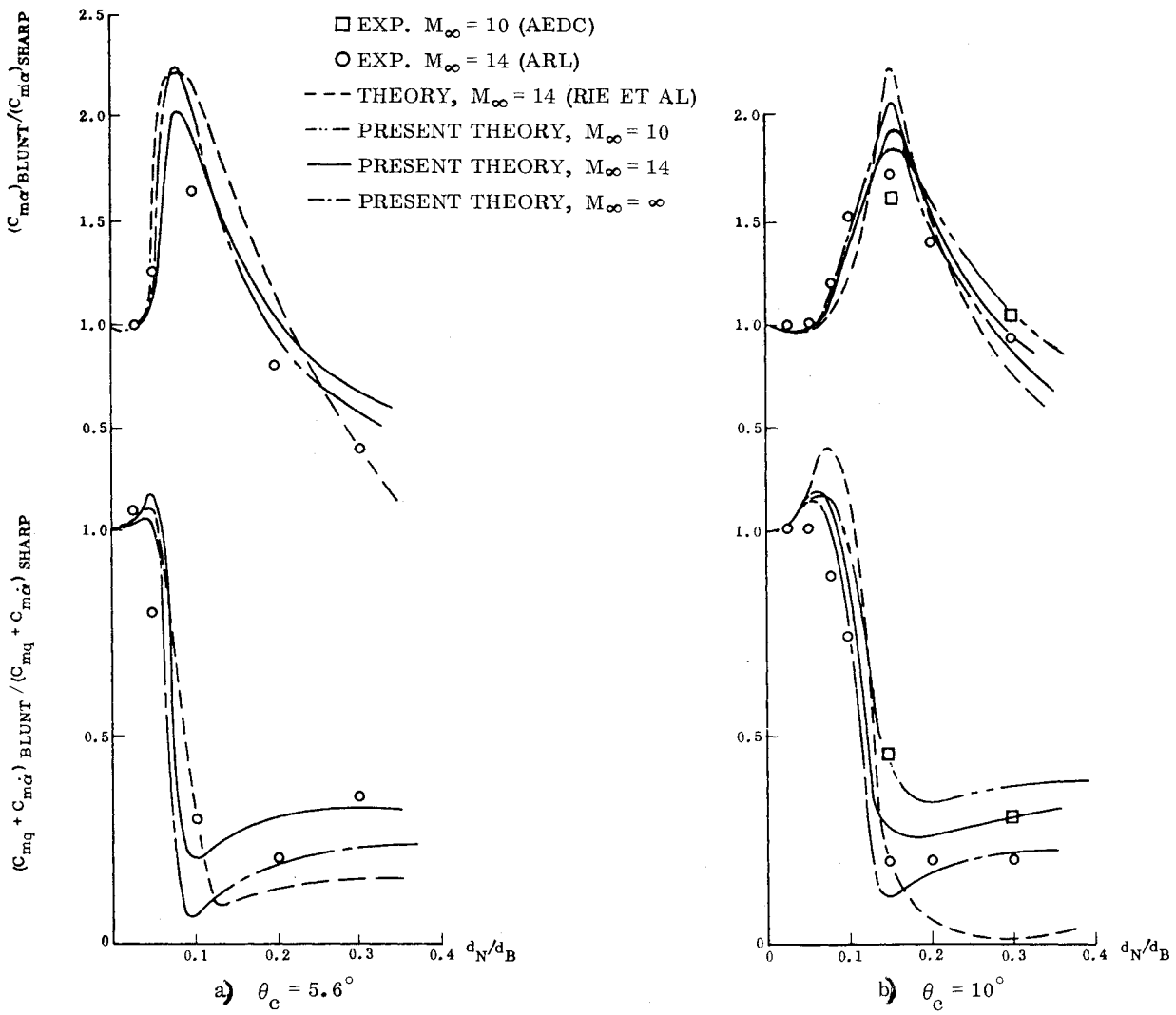

Fig. 6 Predicted and measured stability derivatives of slender blunted cones ($\Delta\bar{x}/\ell = 0.40$).

seen that the stability derivatives of slender blunted cones show sensitivity to Mach number even at Mach numbers above $M_\infty = 10$. However, the effect is probably too small to be discernible from the data scatter in dynamic tests. This is indicated by the comparison with experimental data [15-17] made in Fig. 6. The agreement with experimental data is very good, as good (at least) as for the much more time-consuming numerical flowfield theory of Rie et al.[2] Note that the opposite effect of nose bluntness on static and dynamic stability derivatives is well predicted.

By representing the nose bluntness effect as the fractional change of sharp-cone characteristics, the following advantages are gained: tangent cone methods can be used, even at supersonic Mach numbers, and predictions made by inviscid theory can be compared with viscous experimental data. The justification for this statement is simply that in using this ratio between blunted and sharp-cone characteristics, the inviscid and viscous cross-flow effects that are common to sharp and blunted cones are eliminated. The same is true about sting interference effects, which often plague dynamic wind tunnel tests.[18] Thus, realistic comparisons between inviscid predictions and experimental results can be made as long as nose bluntness has negligible influence on cross-flow effects and sting interference. This would certainly be the case for tests with completely turbulent flow. However, hypersonic testing is usually done in laminar flow with a relatively thick boundary layer, and nose bluntness may significantly influence the viscous effects. Orlik-Rückemann[19,20] has shown that the "boundary-layer-cushioning" effect usually is small on cones, at least for standard c.g. locations. The effect of nose bluntness on viscous cross flow with associated convective time lag effects should also be small as long as boundary-layer transition does not occur on the (aft) body.[21,22] Experiments indicate the effect to be less than 10%. The most difficult problem by far is the effect of nose bluntness on dynamic support interference,[18] especially in the presence of aftbody transition effects.[23] There is experimental evidence[24] indicating that nose bluntness could have a significant effect on sting interference.

Walchner and Clay thoroughly investigated how to minimize support interference so that the effects would not distort their experimental results.[15] Also Ward's data[17] can be expected to be relatively free of sting interference effects.[3] Thus, the comparisons made in Fig. 6 should be valid, indicating that the present analytic inviscid flow theory can adequately predict the effects of nose bluntness on slender-cone stability characteristics. The comparisons made in Figs. 7-10 are equally valid as far as sting interference goes. However, boundary-layer transition effects[21,22] have distorted the low Mach number comparisons somewhat, in the manner described in Ref. 3.

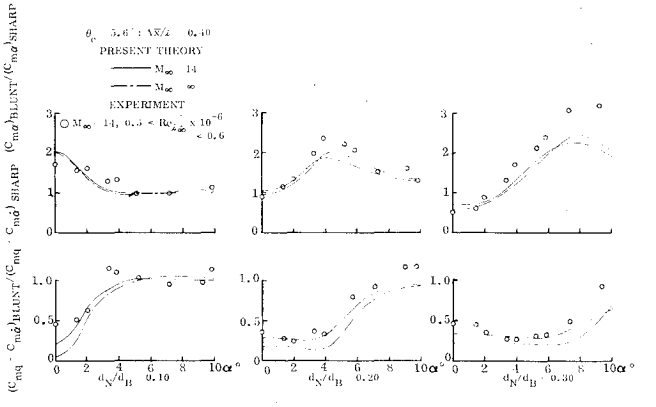

Fig. 8 Comparison between predicted and measured nonlinear stability characteristics of a 5.6° blunted cone at $M_\infty = 14$.

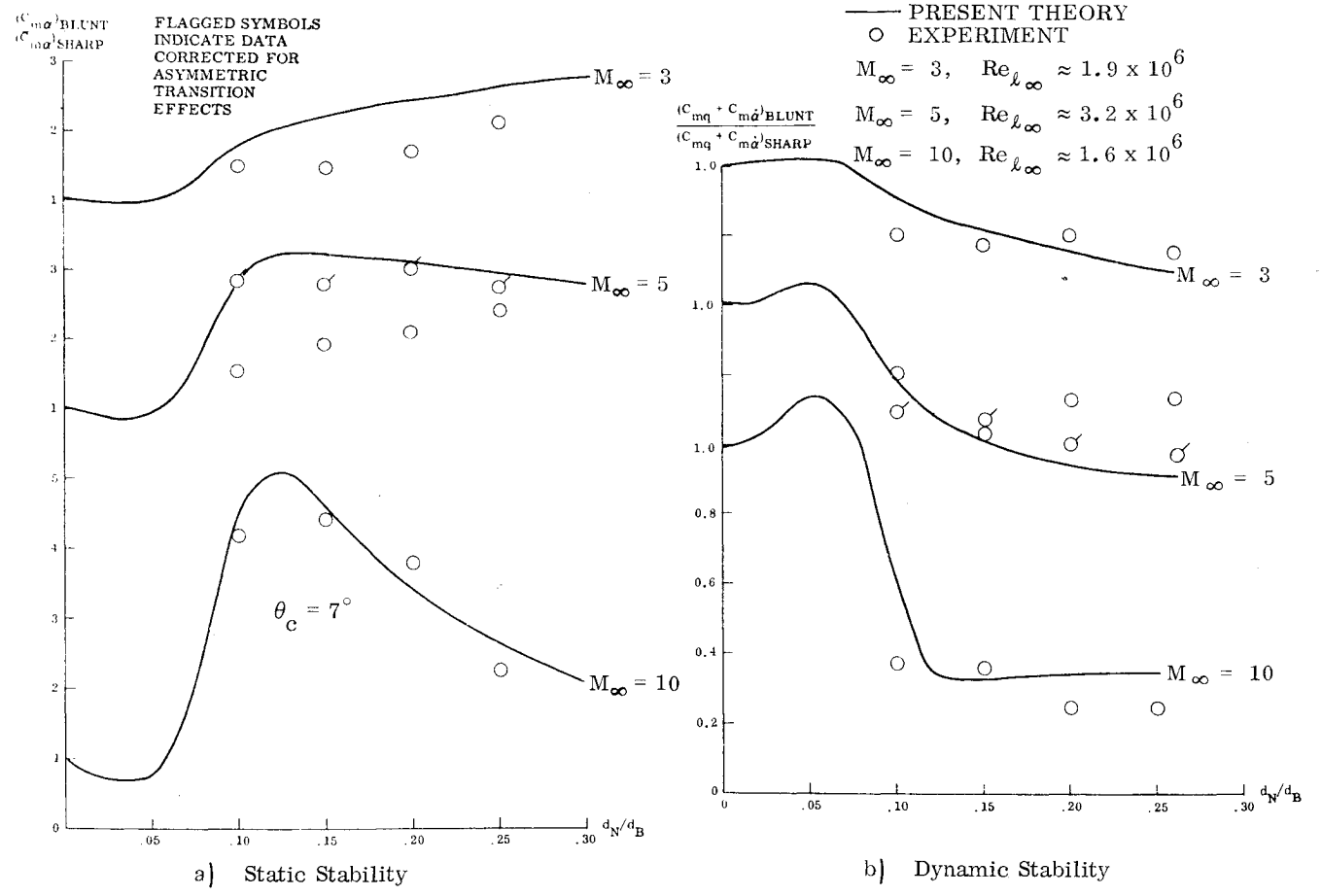

Fig. 7 Comparison between predicted and measured effects of nose bluntness and Mach number on the stability derivatives of a 7° cone.

That the experimentally observed combined effects of nose bluntness and Mach number on static and dynamic stability derivaties are well predicted by the present theory is documented by Fig. 7. The flagged data points have been corrected for boundary-layer transition effects using the total information provided by the stability characteristics at angle of attack for blunted 6°, 7°, and 8° cones (see discussion of Fig. 10).

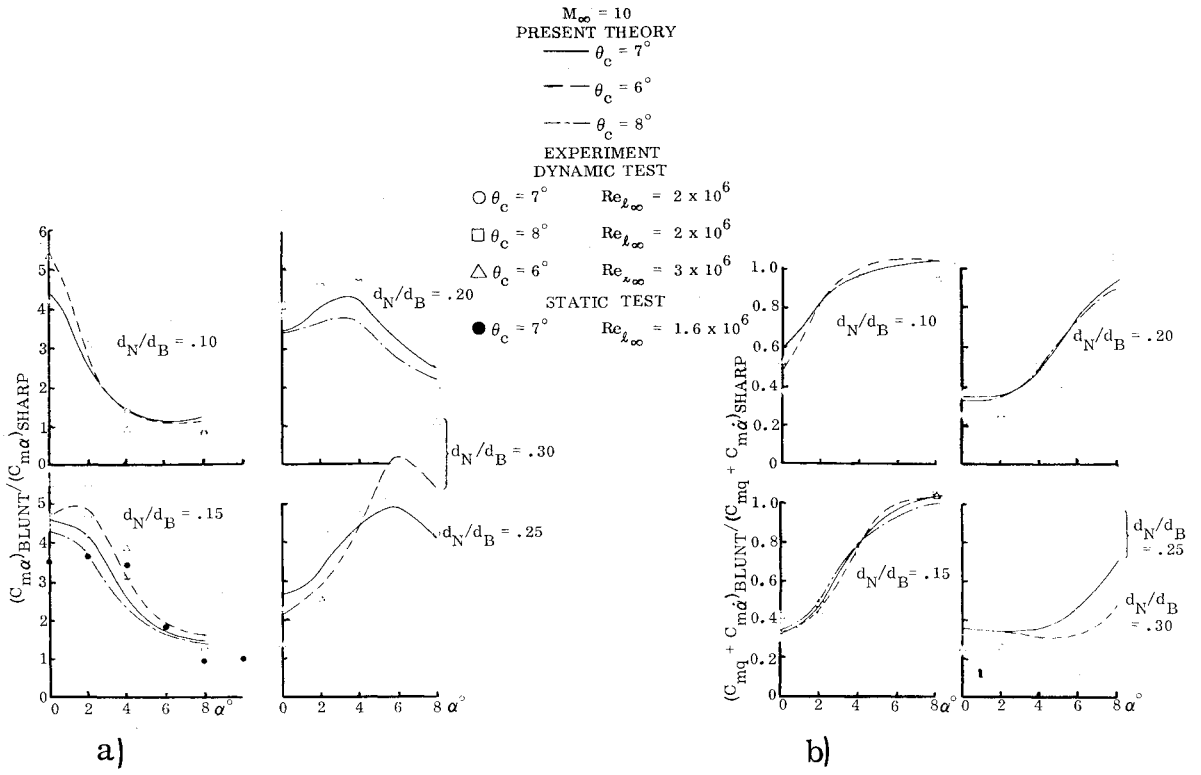

Fig. 9 Comparison between predicted and measured nonlinear stability characteristics of 6°, 7°, and 8° blunted cones at $M_\infty = 10$. a) Static stability; b) Dynamic stability.

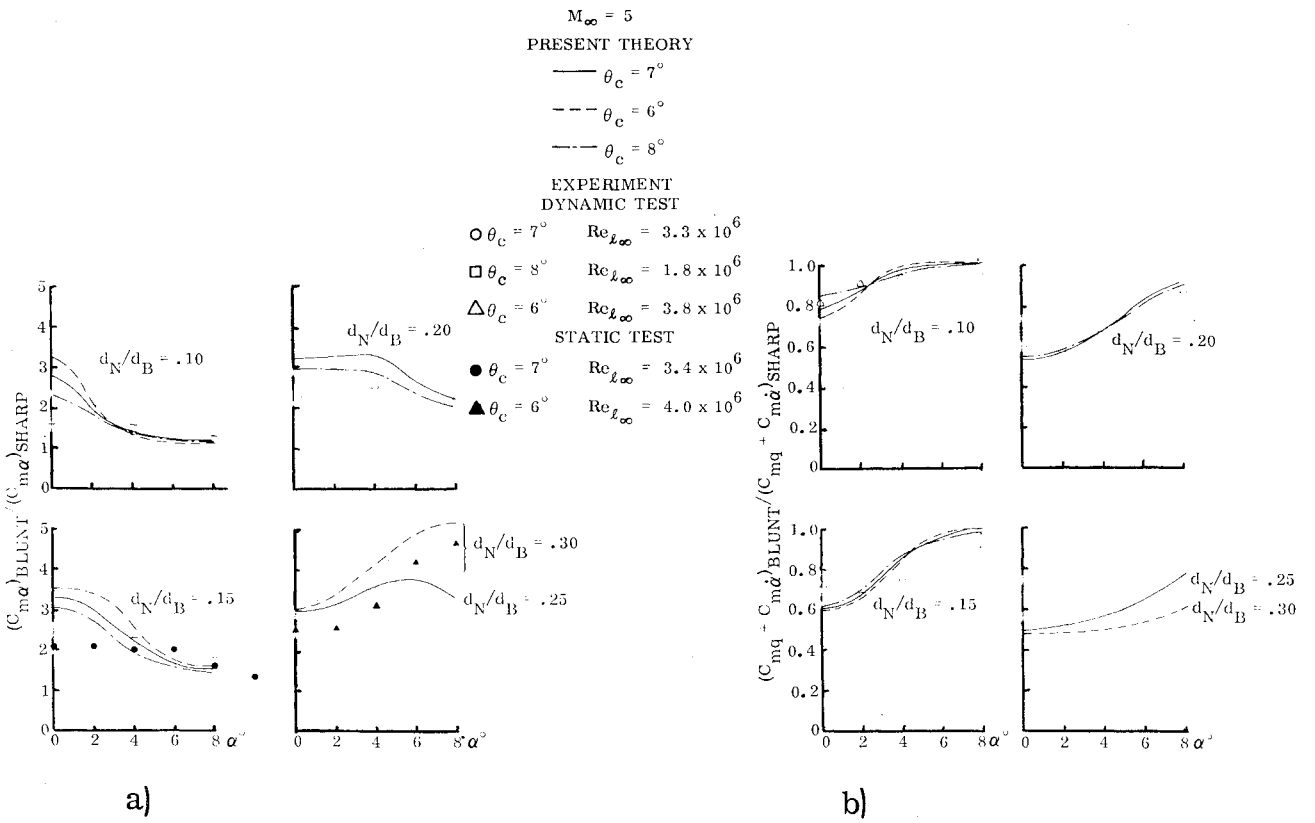

Fig. 10 Comparison between predicted and measured nonlinear stability characteristics of 6°, 7°, and 8° blunted cones at $M_\infty = 5$. a) Static Stability; b) Dynamic stability.

Nonlinear Stability Characteristics

Including the effect of Mach number gives improved damping predictions of the experimentally observed[15] highly nonlinear effects of nose bluntness on a 5.6° cone (see Fig. 8). In addition to the Mach number effect illustrated in Fig. 5, the present method also introduces a steepening of the leeward side entropy gradients for all finite Mach numbers when α/θ_c approaches unity. In Figs. 9 and 10 similar comparisons are made at Mach numbers 10 and 5, respectively. At $M_\infty = 10$, the agreement between present theory and experiment is excellent. (± 10% experimental error in a dynamic test is usually considered small.)

At $M_\infty = 5$ the agreement does at first not appear to be as good at $M_\infty = 10$. (Compare Figs. 10 and 9.) However, the deviations are caused mainly by boundary-layer transition effects.[21,22†] The opposite deviations for static and dynamic stability characteristics are typical for transition effects. It should be pointed out that the sharp cone reference for the experimental data was corrected for transition effects by using the value at $\alpha = 4°$ for $0 \le \alpha \le 4°$ (Fig. 11a). The transition effect on the stability derivatives is usually negligible for $\alpha/\theta_c > 0.5$ (see Refs. 22 and 25). Thus, the deviations in Fig. 10 are caused by transition effects on the blunted cone stability characteristics. Fortunately, the tests cover a sufficiently large range of cone angles and freestream Reynolds numbers to assure that some data free of transition effects are obtained at all bluntness ratios, e.g., $d_N/d_B = 0.10$, 0.15, and 0.20 for $\theta_c = 8°$ and $d_N/d_B = 0.30$ for $\theta_c = 6°$. Using the theoretical data in combination with these transition-free experimental results provided the corrected data shown with flags in Fig. 7.

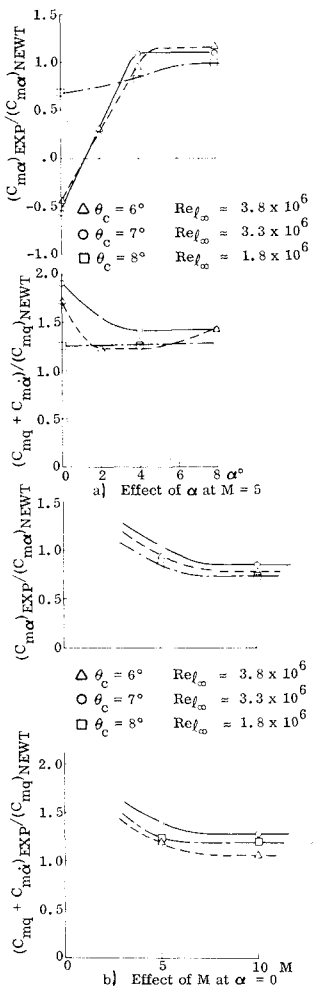

Fig. 11 Comparison between theoretical and experimental sharp cone stability characteristics used as reference levels in Figs. 9 and 10.

The measured effects of boundary-layer transition on sharp-cone stability characteristics are shown in Fig. 11a. The effects are limited to $\alpha/\theta_c < 0.5$ and are of opposite sign in regard to dynamic and static characteristics, all in agreement with documented trends.[21,22,25] Figure 11b shows how the ratio between the experimental and the theoretical (Newtonian) sharp-cone reference levels vary with Mach number. At $M_\infty = 10$, where the boundary layer on the cone is completely laminar, the data trends are in good agreement with the findings of Welsh et al. in their review of available experimental data on sharp or nearly sharp cones.[26] They found a general increase of damping with decreasing Reynolds number, i.e., with increasing boundary-layer thickness. That was true for all ballistic range data. Some wind-tunnel data showed the opposite trend, probably because of interference from the badly designed sting support systems that were used. In the tests producing the experimental data shown in Figs. 7, 9, 10 and 12 great care was exercised to minimize sting interference effects. Consequently, the data at $M_\infty = 10$ in Fig. 11b show the right free-flight trend. That is, the viscous cross-flow effects cause an increase of dynamic stability and a decrease of static stability.

At $M_\infty = 5$ the data are for mixed turbulent-laminar boundary layers from which the distortion due to asymmetrical transition effects has been removed. At $M_\infty = 3$ the data are also for mixed turbulent-laminar flow, but in this case (forebody) asymmetrical transition effects have not been removed. However, based upon past experience, forebody asymmetric transition effects are small for sharp slender cones.[22] The viscous cross-flow effects for the turbulent aftbody boundary layer would also be small, according to Adams' results.[27] Consequently, the data point at $M_\infty = 3$ should be practically free of viscous effects. Using the slender-body value for the experimental damping at $M_\infty = 1$ supplies one "extra" data point, helping to establish the Mach number trends shown in Fig. 11b. Another data point for Mach number effects on inviscid flow characteristics can be obtained from the work of Tobak and Wehrend.[28] They found that $\dot{\alpha}$-effects disappeared at $M_\infty \ge 5.72$, which also happens to be where the experimental data in Fig. 11b lose their Mach number sensitivity.

Thus, the sharp-cone data in Fig. 11b should be fairly representative for full-scale flight. The only question is whether or not the nonnegligible laminar cross-flow effects at $M_\infty = 10$ are representative. They are probably too large. However, this difference between tunnel and flight data is no larger than the probable scatter in the wind tunnel data. The effect of cone angle is inconsistent in Fig. 11b. It can be taken as an indication of the data scatter. Consequently, the curves shown in Fig. 11b represent the best estimate now possible of the full-scale sharp-cone characteristics. In order to obtain the blunted-cone characteristics, undistorted by asymmetric transition effects, one can "extrapolate analytically" from the wind-tunnel data in the following manner. It was shown in Figs. 6-10 that the present theory can predict the experimentally observed large effects of nose bluntness, including the highly nonlinear effects of angle of attack. Hence, the theoretically determined ratios between blunted- and sharp-cone stability derivatives, when multiplied by the sharp-cone characteristics in Fig. 11b, give a realistic estimate of full-scale blunted-cone characteristics (Fig. 12). The figure shows that Mach number has as large an effect on the stability characteristics as the nose bluntness itself. Static stability decreases with increasing Mach number for small nose bluntnesses, whereas the opposite trend is apparent for large nose bluntness. The intermediate nose bluntness for which the Mach number effect on static stability is insignificant is shown as a function of cone angle in Fig. 13. The carpet plot in Fig. 12 could also be used, for example, to select the optimum initial nose bluntness (and cone angle) for a certain

† As stated earlier, the tests are relatively free of sting interference effects.

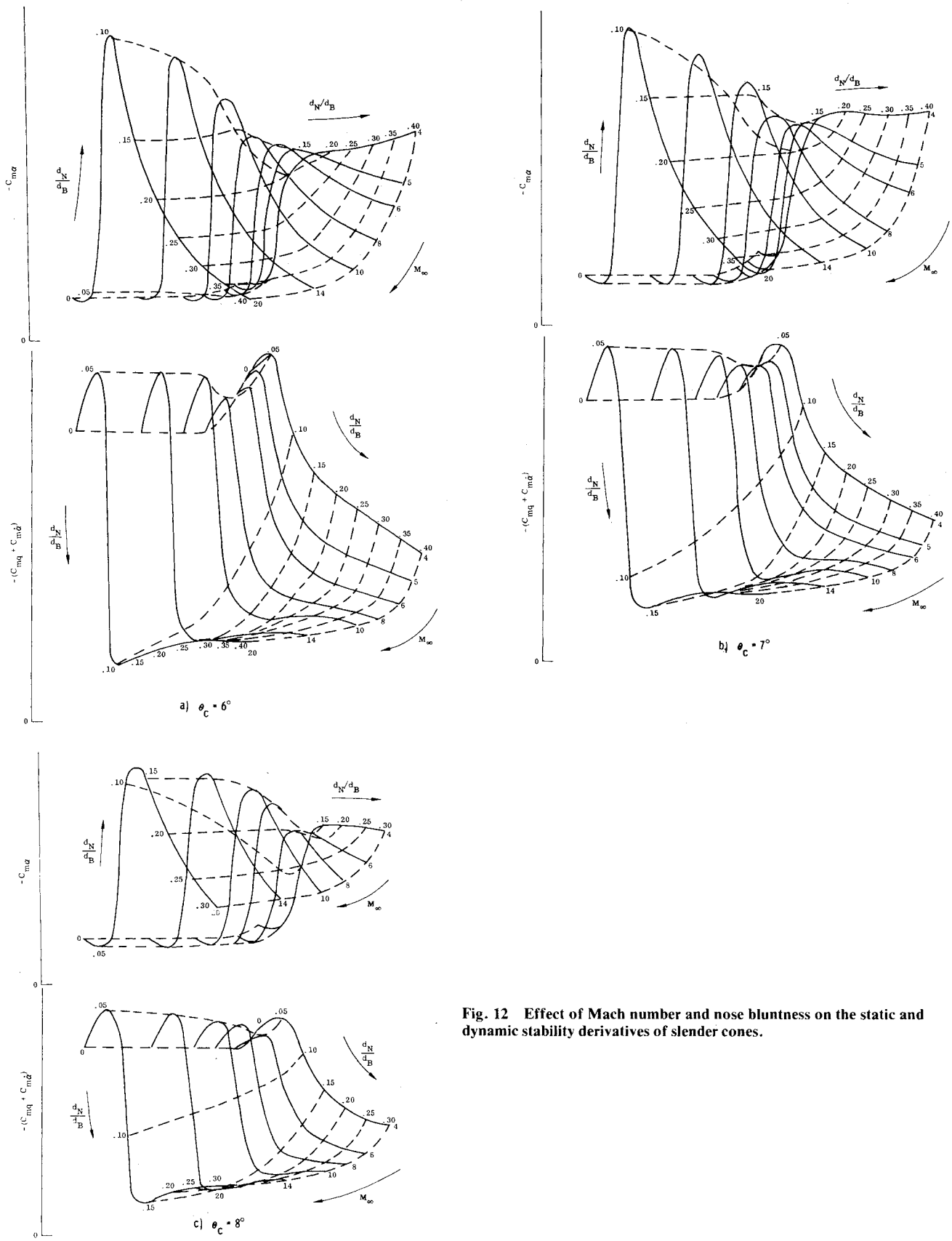

Fig. 12 Effect of Mach number and nose bluntness on the static and dynamic stability derivatives of slender cones.

nose bluntness-Mach number history, as it would apply to an ablating re-entry body.

Conclusions

An analytic theory has been developed for the determination of the effects of nose bluntness on slender-cone unsteady aerodynamics at Mach numbers from $M_\infty = 3$ to $M_\infty = \infty$. The theoretical predictions are in excellent agreement with available experimental data, including the highly nonlinear effects of angle of attack on blunted-cone stability, provided that proper consideration is given to vicous-flow effects. The analysis shows that the effect of Mach number on blunted-cone stability characteristics can be as large as the effect of the nose bluntness itself. However, nose bluntness-

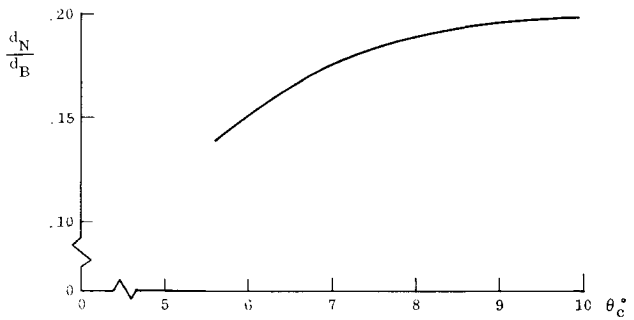

Fig. 13 Nose bluntness-cone angle combinations giving Mach-number-insensitive static stability characteristics.

cone angle combinations exist for which the static stability characteristics become relatively insensitive to Mach number.

References

[1] Hayes, W. D. and Probstein, R. F., *Hypersonic Flow Theory*, Academic Press, New York and London, 1959.

[2] Rie, H., Linkievicz, E. A., and Bosworth, F. D., "Hypersonic Dynamic Stability, Part III, Unsteady Flow Field Program," AFFDL TDR-64-149, Part III, Jan. 1967, Air Force Flight Dynamics Lab., Wright Patterson AFB, Ohio.

[3] Ericsson, L. E., "Unsteady Embedded Newtonian Flow," *Astronautical Acta*, Vol. 18, Nov. 1973, pp. 309-330.

[4] Malcolm, G. N. and Rakich, J. V., "Comparison of Free-Flight Experimental Results and Theory on the Nonlinear Aerodynamic Effects of Bluntness for Slender Cones," *AIAA Journal*, Vol. 9, March 1971, pp. 473-478.

[5] Sieff, A., "Secondary Flow-Fields Embedded in Hypersonic Shock Layers," NASA TND-1304, May 1962.

[6] Sieff, A. and Whiting, E. E., "Calculation of Flow Fields from Bow-Wave Profiles for the Downstream Region of Blunt-Nosed Circular Cylinders in Axial Hypersonic Flight," NASA TND-1147, Nov. 1961.

[7] Sieff, A. and Whiting, E. E., "Correlation Study of the Bow-Wave Profiles of Blunt Bodies," NASA TND-1148, Feb. 1962.

[8] Chernyi, G. G., "Effect of Slight Blunting of Leading Edge of an Immersed Body on the Flow around It at Hypersonic Speeds," NASA TT F-35, 1069.

[9] Cheng, H. K., "Hypersonic Flow with Combined Leading-Edge Bluntness and Boundary-Layer Displacement Effect," Rep. No. AF-1285-A-4 (Contract Nonr-2653(00)), Aug. 1960, Cornell Aero. Lab. Inc., Buffalo, N. Y.

[10] Wagner Jr., R. D. and Watson, R., "Induced Pressures and Shock Shapes on Blunt Cones in Hypersonic Flow," NASA TND-2182, March 1965.

[11] Roberts, J. F., Lewis, C. H., and Reed, M., "Ideal Gas Spherically Blunted Cones Flow Field Solutions at Hypersonic Conditions," AEDC-TDR-66-121, Aug. 1966, ARO Inc., Tullahoma, Tenn.

[12] Maslowe, S. A. and Benson, J. L., "Computer Program for the Design and Analysis of Hypersonic Inlets," Rep. 18079, Aug. 1964, Lockheed Aircraft Corp., Burbank, Calif. (also NASA CR 114344).

[13] Keuhn, D. M., "Experimental and Theoretical Pressures on Blunt Cylinders for Equilibrium and Nonequilibrium Air at Hypersonic Speeds," NASA TND-1979, 1963.

[14] Ames Research Staff, "Equations, Tables, and Charts for Compressible Flow," NACA Rep. 1135, (1953).

[15] Walchner, O. and Clay J. T., "Nose Bluntness Effects on the Stability Derivatives of Cones in Hypersonic Flow," *Transactions of the Second Technical Workshop on Dynamic Stability Testing*, Vol. 1, Paper 8, April 20-22, 1965, Arnold Engineering Development Center, Arnold Air Force Station, Tenn.

[16] Clay, J.T., "Nose Bluntness, Cone Angle, and Mach Number Effects on the Stability Derivative of Slender Cones," ARL 67-0185, Sept. 1967, Aerospace Research Lab., Wright Patterson AFB, Ohio.

[17] Ward, L. K. and Uselton, B. L., "Dynamic Stability Results for Sharp and Blunted 10° Cones at Hypersonic Speeds," *Transactions of the Third Technical Workshop on Dynamic Stability Problems*, Vol. III, Paper 2, Nov. 4-7, 1968, NASA Ames Research Center, Moffet Field, Calif.

[18] Reding, J. P. and Ericsson, L. E., "Dynamic Support Interference," *Journal of Spacecraft and Rockets*, Vol. 9, May 1972, 547-553.

[19] Orlik-Rückemann, K. J., "Dynamic Viscous Pressure Interaction in Hypersonic Flow," Aeronautical Report LR-535, July 1970, National Research Council of Canada, Ottawa.

[21] Ericsson, L. E., "Effects of Boundary-Layer Transition on Vehicle Dynamics," *Journal of Spacecraft and Rockets*, Vol. 6, Dec. 1969, pp. 1404-1409.

[22] Ericsson, L. E., "Transition Effects on Slender-Vehicle Stability and Trim Characteristics," *Journal of Spacecraft and Rockets*, Vol. 11, Jan. 1974, pp. 3-11.

[23] Ericsson, L. E. and Reding J. P., "Boundary-Layer Transition and Dynamic Sting Interference," *AIAA Journal*, Vol. 8, Oct. 1970. pp. 1886-1888.

[24] Peterson, C. W. and Bogdonoff, S. M., "Experimental Study of Laminary Hypersonic Blunt Cone Wakes," AIAA Paper 69-174, New York City, June 1969.

[25] Ericsson, L. E., "Correlation of Attitude Effects on Slender-Vehicle Transition," *AIAA Journal*, Vol. 12, April 1974, pp. 523-529.

[26] Welsh, C. J., Winchenbach, G. L., and Madagan, A. N., "Free-Flight Investigation of the Aerodynamic Characteristics of a Cone at High Mach Numbers," *AIAA Journal*, Vol. 8, Feb. 1970, pp. 294-300.

[27] Adams, J. C., Jr., "Finite-Difference Analysis of the Three-Dimensional Turbulent Boundary Layer on a Sharp Cone at Angle of Attack," AIAA Paper 72-186, Washington D. C., Jan. 1972.

[28] Tobak, M. and Wehrend, W. R., "Stability Derivatives of Cones at Supersonic Speeds," NACA TN-3788, (1956).